

Spectroscopy of $z \sim 5$ Lyman Break Galaxies in the ESO Remote Galaxy Survey

L.S. Douglas^{1,2}, M.N. Bremer², M.D. Lehnert¹, E.R. Stanway¹ & Bo Milvang-Jensen³

¹*Laboratoire d'Etudes des Galaxies, Etoiles, Physique et Instrumentation GEPI, Observatoire de Paris, Meudon, 92195 France*

²*H H Wills Physics Laboratory, Tyndall Avenue, Bristol, BS8 1TL, UK*

³*Dark Cosmology Centre, Niels Bohr Institute, University of Copenhagen, Juliane Maries Vej 30, 2100 Copenhagen, Denmark*

Accepted . Received ; in original form

ABSTRACT

We present the global results of a large spectroscopic survey carried out in order to identify $z \sim 5$ Lyman break galaxies (LBGs) across ten widely-separated ~ 45 arcmin² fields to a depth of $I_{AB} = 26.3$. The redshifts of seventy $4.6 < z < 5.6$ LBGs were identified through their Ly α emission and/or a strong continuum break, with thirty eight sources showing detectable line emission of between 2.6×10^{-18} and 7×10^{-17} erg cm⁻² s⁻¹. Just over half of the spectroscopically-confirmed $z \sim 5$ galaxies have rest-frame Ly α equivalent widths above 20 Å, double the frequency of similarly strong line emitters in similar $z \sim 3$ LBG samples. However, when reasonable corrections are made for the spectroscopically-unconfirmed sources that are nevertheless at these redshifts in both samples, we find no significant difference in the frequency of high equivalent-width line emitters between the samples. The rest-frame UV continuum slope of a typical $z \sim 5$ line-emitting galaxy (as measured primarily from photometry, but also apparent in spectroscopy) is bluer than that of a typical break-only galaxy, a difference that is difficult to explain purely by differences in the ages of their stellar populations. Variation in metallicity and/or dust extinction can more straightforwardly account for this difference. If the correlation between metallicity and UV continuum slope identified at low redshift is applicable at $z > 3$, the typical $z \sim 5$ LBGs have metallicities a factor of three lower than those of LBGs at $z \sim 3$. HST imaging of a subset of the LBGs indicates that a large majority of the spectroscopically-confirmed LBGs in our sample are members of multiple systems (on \sim arcsec scales) and/or show disturbed morphology. Using local LBG analogues as a model, this multiplicity could be explained either by super-starburst regions within a larger unseen structure, or by a high incidence of merging events at this epoch. The current data cannot distinguish between these two possibilities. The surface density of $z \sim 5$ LBGs in two of the ten fields is considerably higher than in the rest. Both show clear spikes in their redshift distributions indicating strong three-dimensional clustering in these fields. Against an expectation of about one source per 0.1 in redshift between $4.8 < z < 5.6$, one field has seven identified objects between $5.11 < z < 5.21$ and the other has 17 between $4.95 < z < 5.15$. Neither structure can be bound given their depth in redshift and probably extend beyond the observed fields. The three-dimensional distances between LBGs in the structures are too large for them to have triggered their starbursts through mutual gravitational interaction, and so it is likely that the short-lived LBGs represent only a small fraction of the baryons in the structures.

Key words: galaxies: high-redshift, galaxies: starburst

1 INTRODUCTION

The identification and observational study of the earliest galaxies is crucial to our understanding of how galaxies form and evolve. With increasing cosmic age, increasingly com-

plex physical processes can affect the properties of galaxies. Consequently, it is hoped that the earlier a galaxy is observed, the more straightforward it will be to compare its properties to any theory of galaxy growth. Whether or not this turns out to be true in practice, such galaxies can be

used as markers of early structure formation and explored as candidate emitters of the radiation responsible for reionization.

While several different techniques have been successfully used to identify galaxies at $z > 5$, the Lyman break technique is arguably the most useful as it can provide a sample of objects with measurable properties for individual galaxies (Lyman α line strength, continuum spectral energy distribution and potentially absorption line diagnostics of the sample or of individual objects if bright enough). Optically-selected samples of high redshift Lyman break galaxies (LBGs) are dominated by systems that are undergoing strong and unobscured star formation because by $z \sim 5$ optical observations probe the rest-frame spectral region shortward of 1800\AA , where emission is dominated by comparatively short-lived O and B stars.

In this decade there has been considerable progress in the observational identification of systems at these redshifts. This has allowed us to take the first steps towards understanding the properties of galaxies that most likely represent the earliest stages in the evolution of current-era massive galaxies (e.g. Verma et al. 2007). Thousands of candidate $z \sim 5$ star forming LBGs have been identified in large-area ground-based photometric surveys, but only a very small fraction of these have been confirmed spectroscopically. While studies of optically-selected photometric samples can provide reliable insights into the properties of the sources when HST imaging is used on its own or in combination with deep infra-red photometry (e.g. Bouwens et al. 2007; Verma et al. 2007), deriving reliable conclusions from ground-based optically-selected samples is more problematic. Not only do these samples suffer from the effects of contamination (see e.g. Stanway et al. 2008b; Douglas et al. 2009, hereafter paper I), but the information supplied on each system is minimal and so their detailed properties cannot be explored.

Spectroscopically-confirmed samples of $z \sim 5$, while inevitably smaller than photometric samples, ultimately allow more detailed studies of the properties of the galaxies. With a reliable sample, uncertainties in statistical properties such as the luminosity function can be minimised. Correlations between observables, such as line-strength and colour, start to unravel the evolution of the objects. Instead of exploring the clustering by statistical methods in two dimensions (which can be unreliable if the sample is contaminated), a direct determination of three-dimensional clustering can be made. With the stochastic and relatively short-lived nature of the star formation within these systems, the interpretation of clustering is potentially complicated given that the timescale over which a source may be UV-luminous can be only a small fraction of the look-back time through a survey volume. The most important benefit of a spectroscopically-confirmed sample is that it allows further spectroscopic follow-up in other wavebands (e.g. Stanway et al. 2008a), so will eventually lead to a fuller understanding of the early stages of galaxy formation and evolution.

In order to furnish ourselves with a sample of objects with which to carry out such studies, we have carried out a spectroscopic survey of ten widely-separated $\sim 45 \text{ arcmin}^2$ fields as part of the ESO Remote Galaxy Survey (ERGS), an ESO large programme (PI M. Bremer, ID 175.A-0706) in order to identify and spectroscopically-confirm a sample of

$z \sim 5$ unobscured star-forming galaxies. We had several motivations for carrying out this spectroscopic survey. Firstly, to explore the reliability of photometric samples and how they impact the reliability of statistical properties for $z \sim 5$ LBGs, e.g. their luminosity function (see paper I). Secondly, to obtain as large a sample of confirmed $z \sim 5$ LBGs as possible in a reasonable amount of time (the aim being at least 50 $z \sim 5$ LBGs in 100 hours of 8m spectroscopy). A sample of this size (especially when combined with other published samples) allows exploration of the properties of the sources and of any correlation between them. Thirdly, by obtaining such a sample over multiple widely-separated pointings, 3-dimensional clustering can be explored directly, without being dominated by cosmic variance in any one field.

The structure of the paper is as follows. In section 2 we describe the data and sample selection of high redshift LBGs. Details and examples of spectroscopic identification are given in section 3. Discussion of the global properties of the sample follows in subsequent sections. The $z \sim 5$ redshift distribution is described in section 4. Section 5 explores the rest-frame UV continuum of the LBGs and in section 6 the properties of the observed Ly α emission are discussed. In section 7 we describe the morphology of the confirmed high redshift LBGs. The surface density of sources is discussed in section 8 and the results of the $z \sim 6$ LBG search are presented in section 9.

We adopt the standard Λ CDM cosmology, i.e. a flat universe with $\Omega_\Lambda = 0.7$, $\Omega_M = 0.3$ and $H_0 = 70 \text{ km s}^{-1} \text{ Mpc}^{-1}$. All photometry was determined in the AB magnitude system (Oke & Gunn 1983).

2 DATA AND SAMPLE SELECTION

2.1 Imaging Data

The spectroscopic sample was derived from the same set of imaging data used to derive the photometric sample previously presented in paper I. The data included deep (around two hours per band) V , R , I and z -band imaging obtained with FORS2 (Appenzeller et al. 1998) on the VLT and moderately-deep J and K_s -band imaging (5-6 hours per band) obtained with SOFI on the NTT. The optical data covered approximately 49 arcmin^2 in each field, while the near-IR data covered approximately half the area of the optical data per field. While the photometric sample reported in paper I was drawn from 286 arcmin^2 requiring both optical and near-IR coverage, the spectroscopic candidates were drawn from an effective area of 440 arcmin^2 , the area covered by the R and I -band imaging after taking into account the area compromised by high surface brightness foreground objects. All imaging except the z -band frame were obtained as part of the ESO Distant Cluster Survey (EDisCS), itself an ESO large programme (PI S. White, ID:166.A-0162, see White et al. 2005). The z_{AB} -band imaging was obtained as part of ERGS. Although there was some field-to-field variation, typical 2σ limits in a $2''$ circular aperture were $V_{AB}=28.1$, $R_{AB}=28.0$, $I_{AB}=27.1$, $z_{AB}=26.0$, $J_{AB}=24.5$, $K_{AB}=23.6$ and seeing varied between $\sim 0.6''$ and $0.8''$ in the optical bands, $0.8''$ and $1.0''$ in J_{AB} and $0.6''$ and $0.8''$ in K_{AB} , comparable to the quality and depth of other surveys of the equivalent or larger area. See paper I for a detailed field-to-field breakdown.

2.2 Spectroscopic Sample

As for the photometric sample discussed in paper I, the primary selection criteria of $I_{AB} < 26.3$, $R_{AB} - I_{AB} > 1.3$ and $V_{AB} < 27.5$ were used to select objects that may have the characteristic spectral break of $z > 4.8$ LBGs. The same SExtractor (Bertin & Arnouts 1996) catalogues were used to select objects for the photometric sample and spectroscopic targets. The photometric sample was generated using 2 arcsec diameter circular apertures so that photometry across all the bands (with different pixel sizes) could be combined in the object selection. While the photometric sample was defined to allow an accurate determination of completeness and contamination, one aim of the spectroscopy was to maximise the number of spectroscopic candidates to be targeted with the slit masks, thereby maximising the size of the spectroscopically-confirmed $z \sim 5$ LBG sample. Consequently, we performed the candidate selection twice using the same criteria with different photometric catalogues. The first catalogue used the aperture magnitudes from paper I and the second used total magnitudes measured using the SExtractor MAG_AUTO apertures defined in I and with appropriate corrections to the V and R -band value (typically of a few hundredths of a magnitude due to the difference in seeing between the bands). If an object satisfied the primary selection criteria in either of the apertures, it was flagged as a candidate for spectroscopy. In addition, as we specifically wanted to both maximise the number of candidates placed on the spectroscopic masks and explore the potentially contaminating populations, we avoided an explicit $I_{AB} - z_{AB}$ colour cut to rule out potential lower redshift interlopers. In designing the observational strategy, we matched the number of masks to be used in any field to the number of objects selected by the primary selection criteria, ensuring that there were generally sufficient slits to observe objects with any $I_{AB} - z_{AB}$ colour. Figure 1 shows the range of colours of the objects observed during the spectroscopy program.

Even with several masks per field, pairs of candidates will compete for space because their positions are such that their dispersed spectra would overlap. Consequently the candidates were prioritised drawing on our previous experience of comparable spectroscopy with the same instrumentation. We had previously observed four adjoining FORS2 fields, searching for $z \sim 5$ LBGs (Lehnert & Bremer 2003, Davies et al. in prep). As a result of this experience we were able to prioritise the candidates based on their likelihood of being at high redshift, as described below. This was done to maximise the number confirmed of $z \sim 5$ LBGs on the masks.

Each candidate was categorised according to its photometry in all bands and if necessary from visual inspection of all of the ground-based images. If the object had $I_{AB} - z_{AB} < 1$, was undetected in the V , J and K_s -band images, and the photometry was in no way influenced by neighbouring objects (affecting the background estimate or the positioning of the aperture), the object was believed to be at high redshift and given the highest priority (noted as priority 1 in Tables 1 and 2). If the object was detected in the V -band, indicating that it may be a lower redshift galaxy or a star, or had potentially compromised photometry due to object overcrowding it was assigned a lower priority (priority 2 in Tables 1 and 2). Sources which were detected in the near-infrared imaging, with colours inconsistent with high

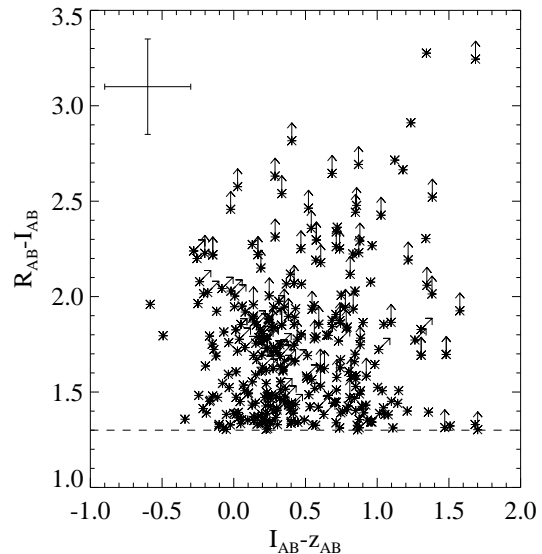


Figure 1. Colour-colour diagram of the spectroscopically observed objects illustrating the range of colours sampled. The dashed line is the formal colour cut used in the photometric selection. Arrows depict where 2σ limits were used.

redshift star-forming galaxies were classified as likely ‘low z ’ objects. Finally, in empty areas of the spectroscopic masks where no other strong candidates could be placed, objects with photometry outside the selection criteria (*e.g.* objects with red $R_{AB} - I_{AB}$ colours but $I_{AB} > 26.3$, objects with $1.0 < R_{AB} - I_{AB} < 1.3$, or objects detected in the V -band) were observed, classified as ‘other’ sources. This was particularly valuable as it probed additional colour space outside the selection. In practice, sufficient objects were observed to obtain good statistics for each class despite slit contention.

Our previous experience had shown that brighter ($I_{AB} < 25$) candidates were almost invariably low redshift galaxies ($0.6 < z < 1.2$) or stars, especially if they had red $I_{AB} - z_{AB}$ or $I_{AB} - K_{AB}$ colours (see paper I for details of the colour modelling of the contaminating populations). However, even in the cases where the multi-band characteristics of an object strongly indicated a low or zero-redshift, an object was not rejected from the list of candidates, merely given a lower priority. This was done so that the reliability of our selection, both for this sample and also for the photometric sample in paper I, could be determined. For objects with $I_{AB} < 25$, it is impossible to rule out with 100 per cent certainty an object being at high redshift based on the ground-based photometry alone; all that can be determined is that an object is highly unlikely to be at high redshift. Objects brighter than $I_{AB} < 24$ selected by our colour cuts would most likely have a strong AGN component in order to be at $z \sim 5$. While our optical colours do not distinguish between a $z \sim 5$ quasar and certain types of late-type stars, given that we detected only a single fainter object with a moderate AGN component in our sample (see Douglas et al. 2007), it is likely that no brighter AGN existed in the volume probed by the survey.

As the near-IR data did not cover all of the optical

fields, the full prioritisation could not be carried out uniformly across all areas. This resulted in less rigorous prioritisation in a fraction of each field. Fortunately, objects which were near-IR detected and therefore less likely to be at the highest redshifts tended to be the brighter objects in the optical, or had red $I_{AB} - z_{AB}$ colours, both of which factors downgraded their priority on their own. Thus a lack of near-IR data did not dramatically change the prioritisation of objects between the regions with and without near-IR data. As prioritisation was only important when there was contention between candidates for space on the slit masks, many candidates were observed regardless of their priority. Table 1 shows the fraction of high and low redshift targets which were observed. The results in table 2 (discussed below) confirm *a posteriori* that the prioritisation was effective.

In addition to the $z \sim 5$ target selection, our data allowed us to select $z \sim 6$ candidates using a redder $I_{AB} - z_{AB} > 1.3$ colour cut which at $z_{AB} > 24.5$ will select LBGs at $z > 6$ (e.g. Stanway et al. 2004). Such objects will not be detected in our near-IR imaging, or in the V -band image. These higher redshift LBG candidates were rarer than those at $z \sim 5$. There were typically nine such candidates per field and a total of 73 candidates were observed on the masks, placed in regions where they did not compete for space with the highest priority $z \sim 5$ candidates.

2.3 Observations

Twenty VLT/FORS2 ‘MXU’ spectroscopic masks were used to obtain redshifts in the ten fields. The number of masks assigned to each field broadly reflected the number of high priority $z \sim 5$ candidates. The only exception is that the field of J1103.7 received an extra mask at the expense of field J1216.8 because the placement of candidates in the latter field made for an inefficient third mask. Each mask was designed to have between 30 to 40 slitlets of width one arcsecond and typical length of 10 arcsec. In general, where two or more candidates contended for space on a slit mask, the highest priority object was chosen. Occasionally, in order to help calibrate the reliability of the photometric sample, a potential contaminant was chosen at random over a higher priority object. For this reason, and because high priority candidates will inevitably contend with each other for space on the mask, not all of the high priority targets had slitlets assigned to them (see table 1).

The observations with FORS2 were carried out in service mode on nights between December 2005 and May 2006. Seeing was always better than 1 arcsec and observations were taken during dark time, clear or photometric conditions and at an airmass below two. The masks were made using *fims*, the mask design software for FORS2 distributed by ESO. Each mask was observed in five blocks of 43 minutes. Each block consisted of four observations of 650 seconds at four different nod positions along the slit resulting in a total on source exposure time of 3.6 hours. These nod positions were also offset between blocks ensuring that the spectrum of each object was placed at 20 independent positions on the CCD. This technique was used to avoid the effects of pattern noise or bad pixels and to facilitate the best possible sky subtraction. FORS2 was used in spectroscopic mode using the 300I grism with the OG525 blocking filter to restrict the wavelength range to between 650-1000nm. The resulting

pixel scale was 3.2\AA in the spectral direction by 0.25 arcsec spatially and the spectral resolution was $\sim 10\text{\AA}$, measured from the width of the sky lines. This observing setup was identical to that used by Lehnert & Bremer (2003) and the choice of grism and blocking filter the same as that used by Vanzella et al. (2005) and Vanzella et al. (2009).

2.4 Data Reduction

The data were reduced following the same standard procedures as those described in Lehnert & Bremer (2003), with the following modifications. The individual spectra were rectified before sky subtraction. As the seeing of the spectroscopic observations was close to (but always less than) the slit width, the spectroscopy did not recover all of the flux of an object. The standard star spectra were taken through a 5 arcsec-wide slit and so recovered a higher fraction of the stellar flux. To account for this, the ratio of flux recovered in $1''$ and $5''$ wide rectangular apertures was measured from I_{AB} -band imaging of standard stars, and the fluxes determined in the spectroscopy were corrected by the factor appropriate to the seeing of the individual exposures. The correction factors typically ranged from 1.1 to 1.5. The final combined exposures reached a flux limit of a few $10^{-18} \text{ ergs cm}^{-2} \text{ s}^{-1} \text{ \AA}^{-1}$ for an unresolved emission line in a dark region of the sky spectrum, comparable to the depth obtained by Lehnert & Bremer (2003) as expected given the identical observational setup (exposure time, grism, slit width).

3 SPECTROSCOPIC IDENTIFICATIONS

The reduced spectra were examined by four of the authors (LSD, MNB, ERS and MDL) and classified into high redshift, low or intermediate redshift and low signal-to-noise categories. The high redshift sources were expected to show a clear continuum break at the redshifted wavelength of $\text{Ly}\alpha$, often with a $\text{Ly}\alpha$ emission line at the same wavelength. Low or intermediate redshift objects were identified through multiple emission lines (such as $\text{H}\beta$ and $[\text{OIII}]$), no break in the continuum or a steeply reddening continuum with molecular absorption bands indicative of low mass stars (Stanway et al. 2008c). Low redshift objects were also identified by the presence of continuum emission at the bluest wavelengths ($\sim 6500\text{\AA}$), inconsistent with a red $R_{AB} - I_{AB}$ colour and therefore included in the sample due to photometric uncertainty. Any spectra exhibiting one or more of these features were classified as low redshift. The object did not necessarily have to have a secure redshift, merely that the spectrum was clearly inconsistent with that of a high redshift LBG. Objects where the signal-to-noise in the continuum was too low to be placed in either of the above categories were classified as ‘unknown’.

In addition to categorising an object as being at high redshift ($z \sim 5$), we split this category into two grades: A and B. If the spectrum was clearly that of a high redshift object with an emission line at the wavelength of a continuum break, or a clear continuum break with no other obvious low redshift features red-ward or blue-ward of the break, the spectrum was classified as grade A. The redshift was determined to the resolution limit of the spectrograph,

Table 1. The number of targets which were observed spectroscopically in the full optical field of view. Targets include high redshift candidates divided into priority 1 and 2 (see text) and likely lower redshift candidates which obey the optical selection criteria but are detected in the near-IR imaging. For each field, the number of photometrically selected targets and the number observed on mask are given for each target category.

Field	No. masks	Priority 1 targets	Priority 1 $z \sim 5$ on mask	Priority 2 targets	Priority 2 $z \sim 5$ on mask	Low z targets	Low z targets on mask
J1037.9-1243	1	7	5	8	2	5	3
J1040.7-1155	3	30	24	12	4	12	7
J1054.4-1146	1	7	4	6	3	5	2
J1054.7-1245	5	53	48	27	15	11	4
J1103.7-1245	2	7	5	8	7	3	3
J1122.9-1136	1	8	3	10	4	13	4
J1138.2-1133	1	7	6	8	3	5	0
J1216.8-1201	2	32	9	23	9	11	9
J1227.9-1138	2	14	13	28	11	5	5
J1354.2-1230	2	15	12	12	4	11	9
All		180	129 (72%)	132	62 (47%)	81	46 (57%)

Table 2. Number of galaxies in the full optical field of view confirmed at low or high redshift according to their assumed low or high redshift photometric identification. Rows give the candidate sub-sample designation, columns give the resulting spectroscopic outcome. The percentages in brackets relate to the fraction of the candidate sub-sample resulting in either a high redshift or unknown classification. The low redshift objects are split into those drawn from areas with and without nIR data. The different sub-samples are described in section 2.2

Sample	$z \sim 5$	Low z objects		Unknown (Low S/N)
		with nIR data	no nIR data	
Pri 1	54 (42%)	8	10	57 (44%)
Pri 2	8 (13%)	8	8	38 (61%)
low z	2 (4%)	30	-	14 (30%)
other	6 (5%)	45	17	45 (40%)

$\sim 400 \text{ km s}^{-1}$, depending upon the location of the features. If the continuum break or Ly α emission line was comparatively weak, particularly if these features were located in the spectral regions containing strong skyline residuals limiting the accuracy of the redshift determination to $\sim 1000 \text{ km s}^{-1}$, it was classified as grade B. We visually compared our spectra to the published one and two-dimensional spectra of Vanzella et al. (2009) and found that the quality of our grade A and B spectra are broadly similar to that of similarly classified spectra in their work, even though the details of the classification schemes are not identical.

Over the ten fields, 54 sources were classified as grade A $z > 4.6$ galaxies, 36 of which were clear Ly α line emitters and 18 showed only a Lyman break at the signal-to-noise of our data. A further 16 candidates at $z > 4.6$, but with grade B spectra were confirmed, two Ly α emitters with weak lines and 14 continuum break galaxies. The redshifts of most of these placed Ly α in spectral regions of comparatively high sky noise caused by the strong atmospheric lines. Table 2 lists the number of high and low redshift galaxies which were confirmed within the different candidate sub-samples.

As can be seen in table 2, the vast majority of galax-

ies confirmed to be at $z \sim 5$ were drawn from the highest priority sample. However, a small number of galaxies which had originally been flagged as likely low redshift interlopers were found to be at high redshift. Similarly some objects flagged as likely high redshift galaxies were confirmed to be at low redshift, highlighting the limitations of purely photometric surveys. An accurate redshift for some of the confirmed low redshift objects could not be measured due to low signal-to-noise or featureless continuum, however a $z \sim 5$ LBG identification could be ruled out, usually because of detectable continuum blue-ward of the expected Lyman break at $z \sim 4.6$.

A further six LBGs were identified in the ‘other’ sample with photometry outside of the selection criteria. Three of these have a V -band flux 0.1-0.2 magnitudes brighter than the V -limit (but fulfil the I and $R - I$ selection). Two were fainter than the I -band flux limit by 0.2 and 0.3 magnitudes. The sixth galaxy had a $R_{AB} - I_{AB} = 1.03$, bluer than the selection limit. This can be explained by the very strong Ly α emission line detected at $z = 4.9$ from this object. At this redshift the line emission falls within the boundaries of the R -band filter, reducing the observed flux difference between the R and I -bands (see Stanway et al. 2008b).

3.1 Example spectra

Figure 2 shows an example of a $z = 5.5$ galaxy. At the centre of the 2D spectrum there is clear evidence of continuum emission with a break across an emission line, a signature of Lyman α at high redshift. The continuum break and emission line can also be clearly seen in the one-dimensional spectrum. The relatively noisy vertical features in the 2D spectrum are residuals from the subtraction of OH atmospheric sky emission. Small-scale apparent continuum features seen in the spectrum can all be accounted for by the sky lines, atmospheric absorption or noise.

Figures 3 and 4 show examples of low redshift contaminants: an intermediate redshift emission line galaxy and a cool star. Several strong emission lines are seen in figure 3 as well as detected continuum at the blue end of the spectrum. The line emission was identified as H β λ 4861, and the

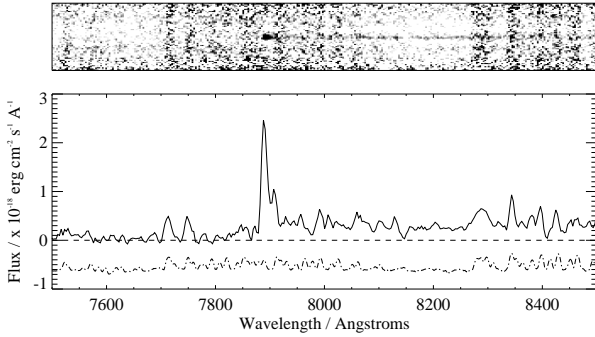


Figure 2. Example of a high redshift galaxy at $z = 5.5$. The top panel shows the reduced two dimensional spectrum where the horizontal direction is wavelength and the vertical direction is the spatial distance along the slit. The bottom panel shows a 1D extraction from the flux calibrated spectrum and the typical atmospheric emission at these wavelengths.

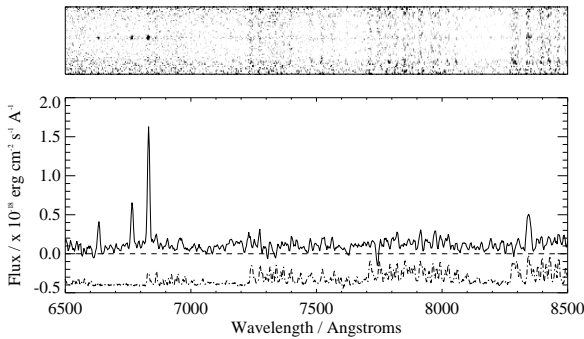


Figure 3. Example of a low z emission line galaxy with $H\beta$ and the $[OIII]\lambda\lambda 4959, 5007$ doublet at $z = 0.36$. Format as described in figure 2.

$[OIII]\lambda\lambda 4959, 5007$ doublet placing the galaxy at a redshift of $z = 0.36$.

The stellar spectrum in figure 4 shows a gradual increase of continuum into the red, no break, and strong molecular absorption bands at 7700\AA , 8500\AA and 9300\AA . At fainter magnitudes spectra like this may look like a continuum source with a strong break so extra care must be taken when identifying Lyman break galaxies without line emission. It is more likely that they will appear as a noisy continuum source which is comparatively strong at the red end of the spectral range, gradually becoming fainter with decreasing wavelength. In this case the source would be spectroscopically classified as ‘unknown’

Further examples of two-dimensional spectra of line emitting and break-only galaxies can be seen in figures 5 and 6.

4 REDSHIFT DISTRIBUTION OF CONFIRMED $Z \sim 5$ GALAXIES

The redshift distribution of all the spectroscopically-confirmed $z \sim 5$ ERGS sources is shown in figure 7. The solid line represents the predicted redshift distribution of the candidates given the photometric selection criteria, depth of

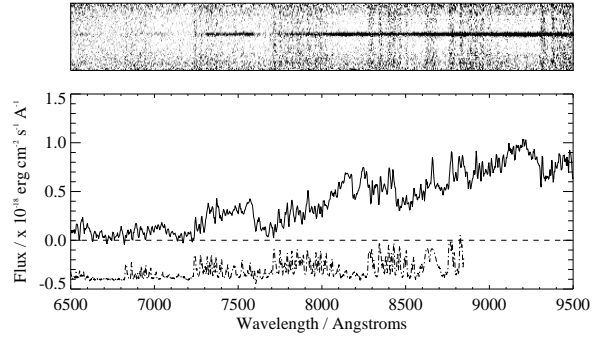


Figure 4. Example of an M-type dwarf star (also see Stanway et al. 2008c). Format as described in figure 2.



Figure 5. Two dimensional spectra of a selection of $Ly\alpha$ emitters at increasing redshift with the $Ly\alpha$ emission marked by the circles. The vertical noise features caused by sky line residuals are clearly seen but do not appear to significantly effect the detection of emission lines. As these spectra have not been rectified for individual spectral distortions, the lower $Ly\alpha$ redshift scale is approximate.

images and the luminosity function of $z \sim 5$ LBGs as determined in paper I. The observed redshift distributions are shown by the dotted and dashed lines. The grade A galaxies are shown by the dashed line and the whole sample of grade A and B objects is shown by the dotted line. The general shape of the observed distributions agrees well with the prediction, indicating that the parameters of the simulations (intrinsic colours of the galaxies, shape of the luminosity function *etc.*) were reasonable. The atmospheric emission, dominated by OH emission lines, at the wavelengths of $Ly\alpha$ for each redshift is plotted below the redshift distri-

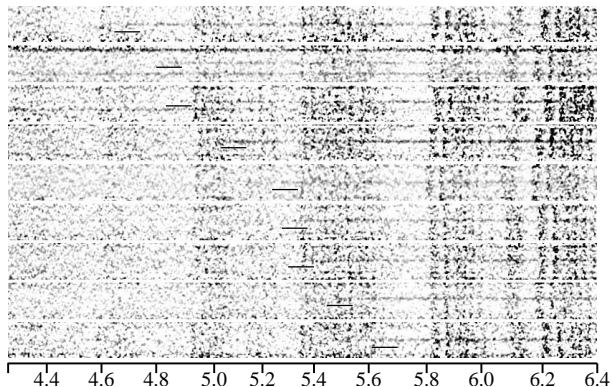


Figure 6. Two dimensional spectra of a selection of Lyman break galaxies at increasing redshift with the location of the break marked by the black lines. Given the faint nature of the objects it can be difficult to clearly display the continuum emission in this format. The vertical noise features are caused by sky line residuals. As the spectra have not been rectified for individual spectral distortions, the lower $\text{Ly}\alpha$ redshift scale is approximate.

butions. Identifying faint high redshift galaxies, especially from breaks alone, in regions of high noise caused by sky line residuals, can be very difficult. For the strong $\text{Ly}\alpha$ line emission and continuum break galaxies (grade A objects) this noise does not have a significant effect, but for fainter sources areas of high noise can seriously hinder any spectroscopic confirmation. This is reflected in figure 7 where the majority of objects with grade B identifications are in areas of high sky signal (and hence large residuals after sky subtraction) with a lower redshift precision ($\sim 1000 \text{ km s}^{-1}$).

Figure 8 shows the redshift distribution of the sample divided into $\text{Ly}\alpha$ line emitting galaxies and continuum-only Lyman break galaxies. Although more line emitters were confirmed, the two distributions span the same redshift range. The presence of line emission does not significantly bias the sample completeness as a function of redshift. Of the 54 grade A spectra, 36 (67%) had $\text{Ly}\alpha$ line emission. The high fraction of confirmed line emitters compared to break-only galaxies is most likely caused by the limited signal-to-noise of the spectroscopy. The redshift of comparatively strong line emitters is much easier to determine than the location of a continuum break. When the whole sample of grade A and B spectra of 70 galaxies is considered 38 (54%) confirmed high redshift galaxies have $\text{Ly}\alpha$ line emission, resulting in a more balanced detection rate for both populations. We stress that a grade B rating does not indicate uncertainty in the high redshift identification, only in the precision of the derived redshift.

5 REST-FRAME UV CONTINUUM SLOPE

In the local universe, the spectral slope in the UV, β (where $F_\lambda \propto \lambda^\beta$), is sensitive to the amount of reddening, the fraction of the non-ionising continuum that is reprocessed into infrared emission, and the metallicity of the galaxy (Heckman et al. 1998). There are good correlations, with similar significance, between the spectral slope and $\log L_{\text{IR}}/L_{\text{UV}}$, the strength of the relatively low ionisation metal lines from the ISM, and the average metallicity. In

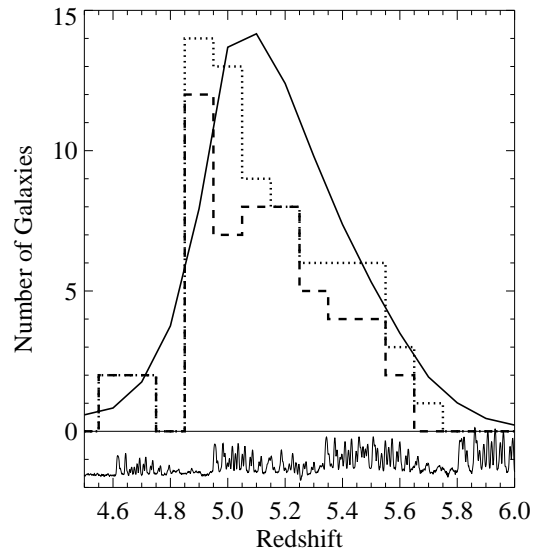


Figure 7. Redshift distribution of spectroscopically confirmed galaxies. The dotted line represents all galaxies with redshifts $z > 4.5$, the dashed line shows only grade A galaxies with secure redshifts and the solid line illustrates the shape of the predicted redshift distribution (scaled to match the peak number count of the observed distribution). Also included, below the distributions, is the atmospheric emission spectrum at the redshift of $\text{Ly}\alpha$.

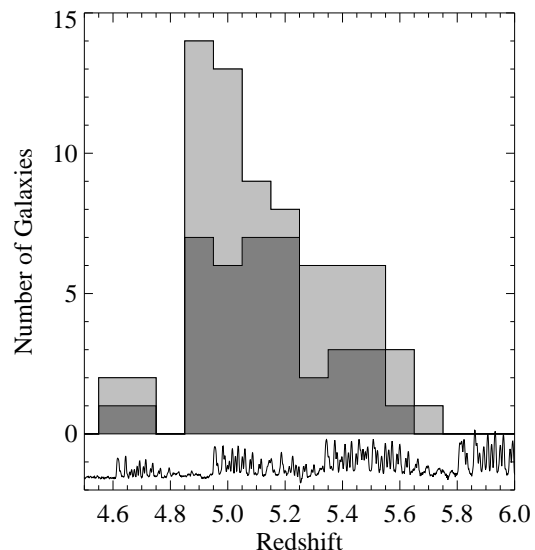


Figure 8. Redshift distributions of $\text{Ly}\alpha$ line emitting LBGs (dark grey) and continuum only LBGs (plotted above the line emitters in light grey). Both grade A and B LBGs are included. Also included, below the distributions, is the sky emission spectrum at the redshift of $\text{Ly}\alpha$.

addition β is relatively insensitive to the age of the galaxy within the first 100 Myrs, lying between -2.6 and -2.0 (Leitherer & Heckman 1995). These correlations reflect the complex relationships between the population of stars that emit significantly in the non-ionising UV (dominated typically by B-stars but is a strong function of age for the youngest populations, *e.g.*, Meurer et al. 1997), the overall extinction and reddening, and the metallicity of the gas (which influences the gas to dust ratio, the gas temperature and ionisation state, and the metal line absorption strength). These relationships can be used to investigate the likely properties of our distant galaxy sample. We can also test the appropriateness of these local relationships by making a comparison with $z \sim 3$ LBGs.

5.1 UV slope from spectroscopy

Two simple average spectra were created, one for the Ly α emitting sources and one for the break-only LBGs, by combining the sources with the best signal-to-noise continuum detections just longward of 1216\AA in the rest-frame using redshifts determined by the location of the continuum break and line emission. A one-dimensional spectrum was extracted from each two-dimensional flux calibrated spectrum, converted to a rest-frame wavelength scale and combined with similar spectra of other galaxies with or without line emission. Spectra of ten sources were combined to form the average line-emitter spectrum and thirteen for the average break-only spectrum. The difference in the number of spectra used for each average affects the signal-to-noise, but not the normalisation or shape of the final spectra. The two sets of sources had comparable redshift distributions, average I -band magnitudes and signal-to-noise at $\sim 1250\text{\AA}$ in their rest-frame spectra. All spectra were drawn from the same sets of masks and identically reduced with the same calibrations; there was no way of determining *a priori* whether an object would be a line-emitter or a break. While the line-emitters were identified from the presence of both a line and break, the identification of the break-only sources required a clear continuum break across 1216\AA , rather than a gradual fading towards the blue and so could potentially bias the highest signal-to-noise break-only sample used here to those galaxies with the bluest breaks.

A comparison of the rest-frame UV slope for the two LBG populations is shown in figure 9. Although this comparison indicates that break-only galaxies have a slightly redder continuum than the line emitters (and show a difference in the opposite sense to the potential bias noted above), this could be due to the Ly α absorption or broad dust features rather than the intrinsic slope of the continuum. Without near-infrared spectroscopy, sampling longer wavelengths, reliable measurements of the UV slope cannot be made with this data. However, at the resolution and wavelength coverage of the $z \sim 5$ spectra presented here, both stacks are consistent with similar stacks of line-emitting and break-only $z \sim 3$ LBGs in Shapley et al. (2003).

5.2 UV slope from photometry

Previous studies have used $I-z$ colours (*e.g.* Pentericci et al. 2007), in the absence of suitable spectroscopy, to measure

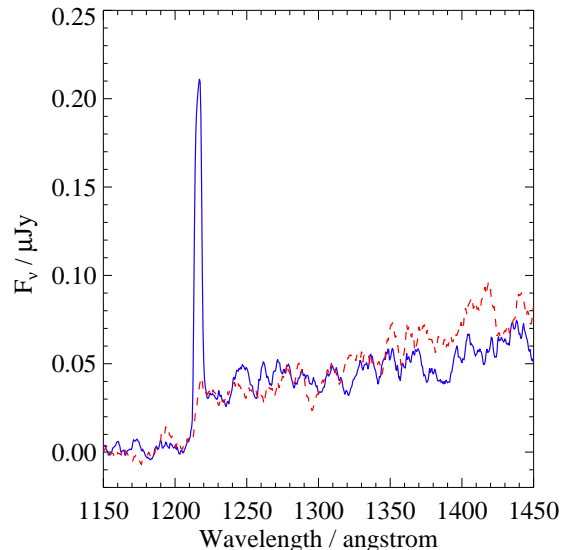


Figure 9. Average spectra of line emitting (solid line) and break-only galaxies (dashed line) smoothed using a boxcar algorithm with a width of 5\AA . The averages were made from spectra of the 10 grade A line emitters and 13 grade A break galaxies with the highest S/N continuum detections just longward of rest-frame 1216\AA , the two sets of galaxies with similar redshift distributions and average I -band magnitudes.

the slope of the rest-frame UV continuum of LBG galaxies at $z = 3-5$. At $z \sim 5$, the ERGS z -band imaging (and spectroscopy) does not provide a wavelength baseline (rest-frame 1200\AA to 1450\AA) sufficient for estimating the continuum slope reliably. Instead, the longer wavelength K_s -band data is used in combination with the I -band, resulting in a rest-frame wavelength range of $\sim 1300\text{\AA}$ to $\sim 3500\text{\AA}$. Although the near-infrared data in this study is not deep enough to detect individual high redshift galaxies, using the technique of stacking many objects together enables the data to reach fainter magnitudes.

Sections of the K_s -band images, centred on the objects of interest, were stacked together using *imcombine* within the *IRAF* package. The mean stack was created with percentile clipping and was then used to measure the average K_s -band flux. Two examples of the LBG stacks are shown in figure 10, the Ly α line emitting and break-only samples. At $z \sim 5$ the Lyman break falls into the I -band which affects the measurement of the continuum level. To correct for this effect and obtain a colour which represents only the continuum, the I -band magnitude of each galaxy contributing to the stacks was corrected for the redshift dependent continuum break effect and Ly α line emission. This gives an average $I_{AB} - K_{AB}$ colour for the whole sample which can be transformed into a measure of the UV to blue optical spectral slope. Table 3 summarizes the stacking of the K_s -band imaging data of spectroscopically confirmed $z \sim 5$ galaxies across the ten survey fields. We found that the break-only galaxies are significantly redder than the line emitters, $I_{AB} - K_{AB} = 0.8$ compared with $I_{AB} - K_{AB} < 0.0$, the 2σ colour limit.

Given the degeneracy between stellar age, reddening

Table 3. Stacked $I_{AB} - K_{AB}$ colour of confirmed high redshift galaxies, break-only galaxies and Ly α line emitting galaxies. The individual I -band magnitudes of the galaxies have been corrected for line emission and the redshift dependent location of the Lyman break within the I -band filter. The rest-frame UV slope is described by β assuming $F_\lambda \propto \lambda^\beta$. Where a limit is shown, the 2σ depth of the stacked K_s -band was used.

Sample	No. gals	I_{mean}	$I_{AB} - K_{AB}$	β
All breaks	20	25.56	0.82 ± 0.23	-1.3
All lines	22	25.62	<0.02	<-2.0
All $z \sim 5$ galaxies	42	25.59	0.27 ± 0.25	-1.8

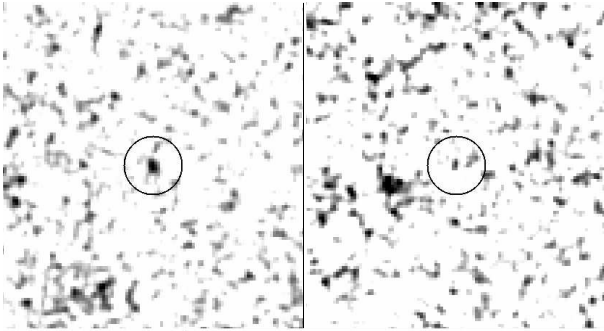


Figure 10. Imaging stacks of the K -band images of break-only galaxies (left), Ly α emitters (right). Both images have the same smoothing and scaling applied.

and metallicity it is difficult to determine the primary source of the observed colour difference between the two subsamples. Nevertheless, we compare the relative effects of stellar age and reddening to the $I_{AB} - K_{AB}$ colour.

Using the Calzetti et al. (2000) dust models, the colour difference between the two subsamples of at least $I_{AB} - K_{AB} \sim 0.8$ can be produced by a small difference in the average reddening between them, with the break-only galaxies being reddened by an extra $E(B-V) \sim 0.2$ relative to the Ly α emitters. The average colours of both samples indicate a low level of dust content, with a typical $E(B-V)$ of more than a few tenths, otherwise the intrinsic colours would be too blue for even very young models with a standard IMF. The levels of reddening are consistent with those found in photometric studies of $z \sim 5$ LBGs (*e.g.* Verma et al. 2007) and in spectroscopic studies of $z \sim 3$ LBGs (*e.g.* Shapley et al. 2003, finds $E(B-V)=0.15$ and 0.1 for break-only and line emitting galaxies at $z \sim 3$).

The colour difference could also indicate an average stellar population age difference between the two subsamples, though any age difference is constrained by the age of the Universe at $z \sim 5$ (about 1.1 Gyr) and, more stringently, with the range of ages found in previous photometric studies of individual $z \sim 5$ galaxies. For example, the study by Verma et al. (2007) used detailed photometry out to $8\mu\text{m}$ to determine that the majority ($\sim 70\%$) of such sources have young (< 100 Myr) dominant stellar populations, with only a minority older than this, typically up to 2-300 Myr.

Using composite stellar population models from

Maraston (2005) that bracket the plausible range of star formation and metallicity for the galaxies, we explored how age differences could affect the observed $I_{AB} - K_{AB}$ colours. For an exponentially declining star formation rate, with an e-folding time of 30 Myr and a metallicity of $0.05Z_\odot$, a colour difference of $I_{AB} - K_{AB} \sim 1$ could be obtained if the youngest subsample was no older than a few 10s of Myr and the oldest ~ 100 Myr older. If the youngest population was itself on average > 100 Myr old, the age difference increases to 200 Myr or more. For a model where the e-folding time was 100 Myr and the metallicity $0.5 Z_\odot$, the older subsample had to be typically 200 Myr older than the younger for almost any plausible age of the younger population out to 500 Myr. For an unreddened $I_{AB} - K_{AB} \sim 0.8$, a source would need to be 200 or 400 Myr old for an e-folding time of 30 and 100 Myr respectively. An unreddened colour limit of $I_{AB} - K_{AB} < 0$ results in ages of < 100 and < 200 Myr for the same models. Associating the line emitters with the youngest populations and the break-only galaxies with the older, the ages of the older populations are difficult to reconcile with the results from Verma et al. (2007), given that half of the spectroscopically-confirmed sample are break-only systems. Clearly it is possible that a combination of differences in both stellar population age and reddening could explain the observed colour difference between the subsamples, but assuming the age constraints indicated by Verma et al. (2007) and the colours of the Maraston (2005) models, the colour difference is more simply achieved through a variation in reddening.

A difference in the intrinsic rest-frame UV continuum slope for LBGs has been seen in other photometric and spectroscopic studies at $z = 3 - 5$. At $z = 3$, UV slopes of $\beta = -0.7$ and $\beta = -1.1$, for break and line emitting galaxies respectively, are measured from spectral stacks in Shapley et al. (2003). Similarly Vanzella et al. (2009) presents a $z \sim 4$ spectral stack for the two galaxy populations which is consistent with the UV slopes measured photometrically in Pentericci et al. (2007) ($\beta = -1.7$ for break galaxies and $\beta = -2.0$ for line emitters). The results presented here follow similar trends with a photometrically measured slope of -1.3 for break-only galaxies and <-2 for Ly α emitting galaxies.

Given that no rest-frame UV colour criteria were used in our observational selection (*e.g.* no $I_{AB} - z_{AB}$ colour cut), the observed targets were not biased to objects with blue continuum. However, the majority of confirmed LBGs were observed to have relatively blue, flat ($\beta \sim -1.8$) rest-frame UV continuum. Only two galaxies were detected individually in the near-IR imaging suggesting a redder continuum. As the objects observed are bright in the UV, it is to be expected that they have blue continuum dominated by young stellar populations. If a sample containing objects with fainter UV luminosities were probed, it would likely contain a higher proportion of older and perhaps more reddened galaxies.

5.3 The Metallicity of $z \sim 5$ LBGs

Heckman et al. (1998) found correlations between the spectral slope and $\log L_{IR}/L_{UV}$, the strength of the relatively low ionisation metal lines from the ISM, and the average metallicity for nearby galaxies. In Figure 11, we plot

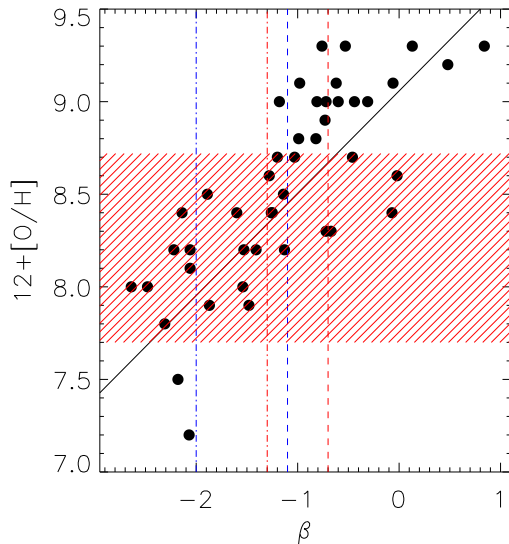


Figure 11. Plot of the UV spectral slope, β , versus the metallicity. The black dots show the spectral slope and metallicity of local galaxies from Heckman et al. (1998), the dot-dashed vertical lines indicate the spectral slope of the galaxies with breaks only in our sample (red) and for the whole sample with spectroscopic redshifts (blue), and the dashed vertical lines indicate the spectral slope of the galaxies with Ly α mostly in absorption (red) and galaxies with Ly α predominately in emission (blue) from Shapley et al. (2003). The red horizontal region shows the area encompassing the metallicity estimates from the literature (see text for details).

the spectral slope, β , versus the metallicity, $12 + \log[\text{O}/\text{H}]$, from the Heckman et al. (1998) sample of local galaxies and their best fit to these data. Overplotted are the estimates of the spectral slope of $z \sim 3$ LBGs from Shapley et al. (2003) and the range of metal abundances determined for $z \sim 3$ LBGs (Pettini et al. 2001; Nesvadba et al. 2006, 2008; Mannucci et al. 2009). Two values of the spectral slope from Shapley et al. (2003) were used, a steeper slope for the Ly α emission line galaxies and a redder slope for the galaxies where Ly α is in absorption.

We see that, in general, β for the $z \sim 3$ LBGs predicts a higher metallicity than has been observed. The number of good metallicity estimates is low and the comparison may suffer from biases (such as slope estimates weighted towards the brightest galaxies, which have populations that are more evolved, or the emission line estimates are weighted towards galaxies of lower metallicities and dust content on average due to the influence of metallicity on the gas temperature, effecting the line strengths of rest frame optical lines). Heckman et al. (1998) found that galaxies brighter in the optical and with higher (approximate) bolometric luminosities have bluer spectral slopes. Realising that in this work we are discussing the brightest LBGs at $z \sim 5$, the spectral slopes suggest that the $z \sim 5$ LBGs are roughly a factor of three lower in metallicity than the $z \sim 3$ LBGs and are approximately 1/5-1/10th of solar metallicity but this estimate may be biased towards galaxies of higher metallicities.

About 10-20% of the LBGs at $z \sim 3$ have stellar ages

consistent with forming at $z \sim 5$. The growth in the number density and in the typical mass of a LBG over this period are also roughly a factor of 10. This may suggest a direct evolutionary connection between the two populations (cf. paper I, Verma et al. 2007; Shapley et al. 2003; Steidel et al. 1999). Moreover, in an analysis of $z \sim 3$ LBGs, Mannucci et al. (2009) find that galaxies with masses similar to those expected for this sample (Verma et al. 2007) have metallicities consistent with our estimates using the measured $z \sim 3$ β and the local relationship between β and metallicity. For such systems, Mannucci et al. (2009) have estimated gas fractions of 80% or more. For the oldest systems at $z \sim 3$, which are also the most massive (see also Erb et al. 2006), the gas fractions are estimated to be much less ($\sim 20\%$). Therefore, although beyond the scope of the present paper, it is possible to relate the more massive, older, more metal-rich populations of LBGs at $z \sim 3$ to the population we observe at $z \sim 5$.

6 LYMAN α LINE PROPERTIES

The Lyman α line is the only emission or absorption line straightforwardly detectable in the observed optical in a reasonable time frame (four hours using a 8m telescope) in the spectra of LBGs at $z \sim 5$. A small number of observations of the continuum of bright or lensed $z \sim 5$ galaxies have reached sufficient depths to probe interstellar absorption features in the rest-frame UV continuum (Ando et al. 2004, 2007; Dow-Hygelund et al. 2005).

6.1 Lyman α at $z \sim 5$

The Ly α line flux of each galaxy was measured within a square aperture centred on the line emission in the two dimensional spectrum. The size of the aperture was tuned to the apparent spatial and spectral FWHM of each galaxy. The flux was integrated over the wavelength range within the aperture, yielding a final measurement in units of $\text{ergs cm}^{-2} \text{s}^{-1}$. Line fluxes ranged from 2.6×10^{-18} to $7.0 \times 10^{-17} \text{ ergs cm}^{-2} \text{s}^{-1}$ (luminosities between 10^{42} and $10^{43} \text{ erg s}^{-1}$) with a typical 3σ line flux limit of $2.9 \times 10^{-18} \text{ ergs cm}^{-2} \text{s}^{-1}$ for an unresolved emission line. At the low redshift end of the sample there is a lack of strong emission lines as a result of the line flux contributing to the R -band magnitude, reducing the $R - I$ colour and causing the object to drop out of the original colour selection. From the $z > 5$ Ly α equivalent width distribution potentially 10-30% of line emitters could be missed at $z < 5$ given the influence of Ly α emission on the $R_{AB} - I_{AB}$ colour (Stanway et al. 2008b).

6.2 Equivalent Width of Ly α

As the observed galaxies are faint ($26.3 > I_{AB} > 25.0$), the continuum emission detected spectroscopically has low signal-to-noise. As such, equivalent width measurements (effectively the ratio of the Ly α line flux to continuum flux density) given here use the broadband photometry of individual galaxies to estimate their continuum flux. Measured line flux was removed from the $2''$ aperture I -band magnitude to determine each galaxy's continuum flux level, accounting for a

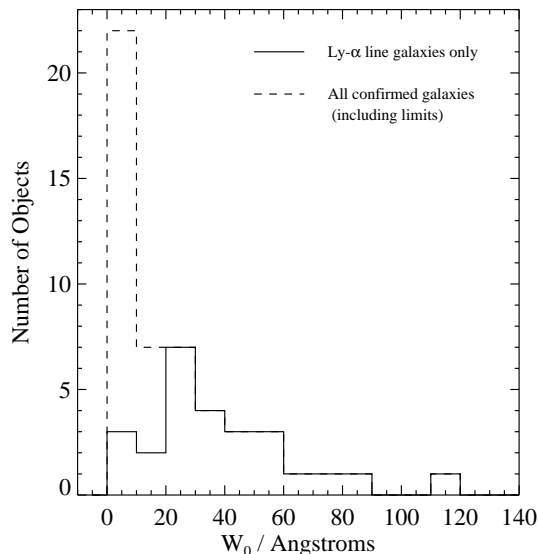


Figure 12. Distribution of the rest-frame Ly α equivalent width for line emitters (solid line) and when 3σ upper limits from spectroscopically-confirmed continuum break galaxies are included as described in the text (dashed line). Continuum flux levels were measured from broadband photometry.

redshift dependent correction due to IGM absorption shortward of Ly α . A limit on the Ly α equivalent width of the break-only galaxies was measured by introducing an artificial line feature with a flux equivalent to the 3σ variations in the local background at the break wavelength. This simulated emission line was placed at the continuum break of the spectrum and used to estimate an upper limit on the observed equivalent width limit which accounted for the noise properties of each spectrum. The derived rest-frame equivalent widths are shown in figure 12. The strongest line detected has a rest-frame equivalent width $W_0 = 112 \pm 18 \text{ \AA}$, the weakest detected line had $W_0 = 6 \pm 2 \text{ \AA}$.

While figure 12 presents the distribution of Ly α line strengths for sources with spectroscopically confirmed redshifts, this is an incomplete picture. To develop a more complete understanding of the equivalent width distribution at $z \sim 5$, it is necessary to consider those sources which were spectroscopically observed, but did not yield a reliable redshift determination or recognisable spectral features. Unsurprisingly, these sources outnumber those with spectroscopic confirmations and must comprise a mixture of faint galaxies, sources at intermediate brightness with weak or absent emission lines, and interlopers contaminating the photometric sample.

In Paper I we determined that $\sim 80\%$ of our refined photometric sample is likely to lie at $z > 5$. Considering a similar subset of sources with reliable multiband photometry, selected as strong high redshift candidates and placed on the spectroscopic masks, we identify 57 sources for which no redshift was determined, of which ~ 45 are expected to be genuine high redshift galaxies, but whose emission lines may lie anywhere in the observed spectrum. In the following we estimate the contribution of the upper limits to any

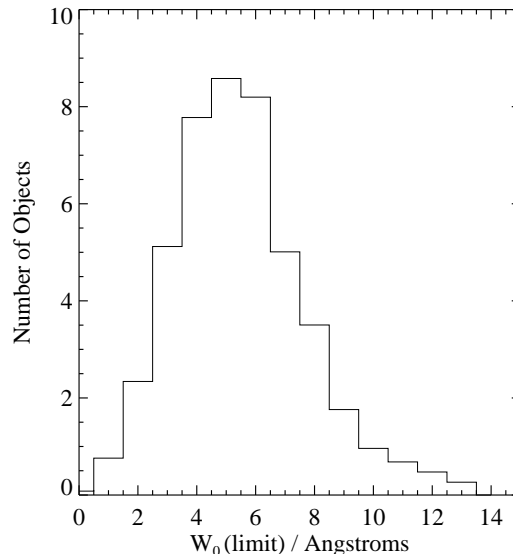


Figure 13. Estimated distribution of rest-frame Ly α equivalent width upper limits for observed sources without distinguishable features in their spectra. This distribution was determined by convolving 3σ upper limits measured from the spectra as a function of redshift with the redshift distribution calculated for the sample, as described in the text.

Ly α emission from these sources to the complete equivalent width distribution.

We calculate a probability distribution of upper limits for this sample as follows. For each source in the sample, we determine a 3σ upper limit on the flux of an undetected emission line as a function of redshift, accounting for wavelength-dependent noise in the spectrum. This is converted to a limit on the rest-frame Ly α equivalent width as a function of redshift, using the I -band magnitude of the source to determine a continuum level (and accounting for IGM absorption shortwards of the proposed emission line, again as a function of redshift). We weight the probability of the line occurring at each redshift by the calculated redshift distribution function of this sample (figure 7), yielding a probability distribution for the 3σ upper limit on the equivalent width for each source. The distribution is then scaled by 80% to produce an estimated contribution to the total sample equivalent width distribution. The resultant distribution of line upper limits is shown in figure 13. The typical 3σ upper limit on a line detection is $5 \pm 2 \text{ \AA}$, with the small amplitude of the tail to higher limits suggesting that our sample is highly complete for line emitters down to our flux limit.

Any interpretation of the Ly α line is challenging given its complex and ambiguous nature. The observed line profile is affected by resonant scattering within the galaxy by interstellar HI. This introduces influences from the geometry, kinematics and dust content of large-scale outflows.

How does the $z \sim 5$ equivalent width distribution compare to that at lower redshifts? At $z \sim 3$, Shapley et al. (2003) determined the equivalent width distribution of Ly α for nearly 1000 galaxies. They find that 25% of $z \sim 3$ Lyman break galaxies have a Ly α equivalent width greater than

20Å. Of galaxies in our spectroscopically-confirmed sample at $z \sim 5$, 55% have $W_0 > 20\text{Å}$. However, when we consider the larger sample of spectroscopically-observed high redshift candidate sources and the estimated contribution of unconfirmed galaxies in figure 13 is taken into account, this fraction falls to $22 \pm 4\%$.

Previous work at lower redshift including Shapley et al. (2003) similarly did not include a correction for unconfirmed sources. While the confirmed fraction at $z \sim 3$ (63%) in that work is significantly larger than that in this sample, and included sources with $\text{Ly}\alpha$ seen in absorption, it is likely that an essentially unknown fraction of the unconfirmed sources would contribute to the $\text{Ly}\alpha$ equivalent width distribution in the same manner as those discussed above. Consequently, the quoted fraction of sources with high equivalent widths at $z \sim 3$ is an upper limit, but nevertheless, even if all unconfirmed sources in the Shapley et al. (2003) sample are at $z \sim 3$, the high equivalent width fraction drops to $\sim 18\%$, consistent with our $z \sim 5$ statistics.

Interestingly, this survey is not alone in finding a large fraction of *confirmed* high redshift galaxies with a large $\text{Ly}\alpha$ equivalent width. A long tail of sources with high equivalent widths is seen by Dawson et al. (2007) at $z = 4.5$, Hu et al. (2004) at $z = 5.7$ and Stanway et al. (2007) at $z \sim 6$, although these studies discuss only sources with spectroscopic confirmation. In contrast Dow-Hygelund et al. (2007) do not observe such a tail based on 6 line emitting galaxies at $z \sim 6$. At present, all of these studies suffer from low spectroscopic completeness and small number statistics. The current study is the first at high ($z > 5$) redshift with sufficient number counts and understanding of selection functions to make a meaningful comparison of the equivalent width distribution to that seen at lower redshifts.

The largest equivalent widths seen at $z \sim 3$ are almost double those at $z \sim 5$. Given their rare occurrence, their absence in the higher redshift sample may simply be an effect of small number statistics. Shapley et al. (2003) also found that the UV continuum slope became bluer as the equivalent width of $\text{Ly}\alpha$ increased in stacked samples of LBGs at $z \sim 3$. Figure 14 shows the distribution of $I_{AB} - z_{AB}$ colour, a rough indicator of the UV continuum slope once corrected for line emission, with the rest-frame equivalent width of $\text{Ly}\alpha$. Although a comparably clear trend is not seen, sources with equivalent widths of more than 30Å appear to have bluer colours than those with lower equivalent widths. There are more z -band detections resulting in redder colours for sources with $W_0 < 30\text{Å}$. However, given the small number of sources this is not highly statistically significant.

The resolution of the spectroscopy was such that only the strongest $\text{Ly}\alpha$ lines were barely resolved, so little can be said about the distribution of line widths and line shapes in the sample; higher resolution spectroscopy is required.

7 MORPHOLOGY OF $Z \sim 5$ LBGs

HST/ACS imaging using the F814W filter (I -band, Desai et al. 2007) were used to investigate the morphology of the confirmed high redshift LBGs (see Douglas et al. 2009, for details). Of the spectroscopically confirmed LBGs, 20 individual sources have deep HST imaging. Within this sample, 14 LBGs have multiple components, four show irreg-

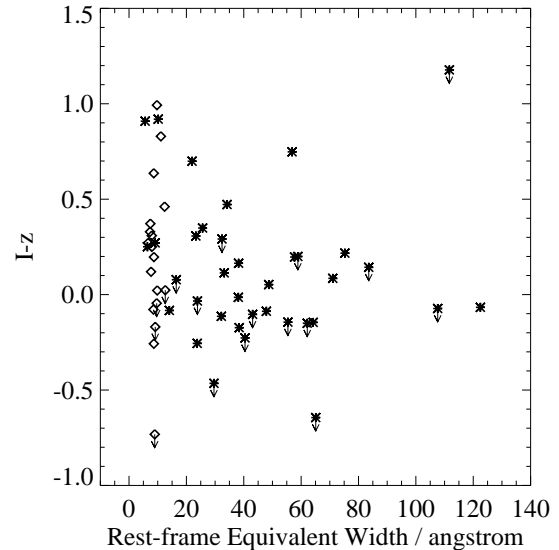


Figure 14. Rest-frame equivalent width of $\text{Ly}\alpha$ as a function of $I_{AB} - z_{AB}$ colour. Diamonds represent equivalent width limits of the break-only galaxies as described in the text. The colour has been corrected for line emission and IGM absorption effects. Arrows indicate a non-detection in the z -band and hence a colour limit.

ular morphology, one is compact and unresolved and the final object is compact but surrounded by diffuse emission. Examples of LBGs with multiple components or irregular morphology are shown in figure 15. The morphology of individual spectroscopically confirmed high redshift galaxies is similar to that of the larger photometrically selected sample of $z \sim 5$ Lyman break galaxies (Douglas et al. 2009). A similar mean half-light radius of $0.15''$ (or 0.9kpc) and distribution of sizes was observed for the two samples, and are in agreement with other high resolution studies (*e.g.* Bremer et al. 2004; Bouwens et al. 2006). The number of components identified in the multiple systems ranged from two to four, however the systems may contain additional fainter components that are not detectable above the surface brightness limits of the images. The mean distance between components is $0.84''$ (5.3kpc) with distances observed between $0.2''$ and $2.5''$ (1kpc and 16kpc) compared to a seeing disk of typically $0.7''$ in the groundbased imaging.

Two systems are resolved in the ground-based imaging with component separations of $0.8''$ and $1.0''$, however further components have been identified in the deeper, high resolution HST images. Within each system, the previously identified components have similar optical colours with no detections in the nIR imaging. Both systems are marginally resolved in the spectroscopy showing two sources. One system has two faint $\text{Ly}\alpha$ emission lines and the other has a line emitter and a break-only galaxy. The component redshifts measured from these features are within 1000 km s^{-1} , which, although high, does not rule out a connected system as redshifts measured using $\text{Ly}\alpha$ emission or the Lyman break are not necessarily equal to the systematic redshift of the galaxy. Velocities of up to 1000 km s^{-1} between $\text{Ly}\alpha$ emission and

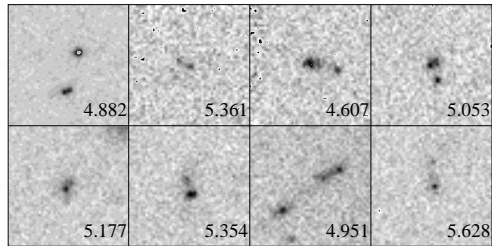


Figure 15. Eight examples of spectroscopically confirmed galaxies with multiple components. Each box is $5'' \times 5''$ and the images were taken using the HST/ACS camera and the F814W filter. Redshifts are indicated in the bottom right-hand corners

interstellar absorption lines have been observed in $z \sim 3$ LBGs.

A higher incidence of complex morphology in the spectroscopically-confirmed sample is observed compared to the larger photometric sample where $\sim 30\%$ of galaxy candidates had more than one component or irregular morphology. This effect has not been observed in other spectroscopically confirmed samples (Vanzella et al. 2005, 2009). However, given the small number of spectroscopically confirmed $z \sim 5$ LBGs and differences in selection and image depths, these numbers are statistically consistent with other studies (Vanzella et al. 2005, 2009; Conselice & Arnold 2009).

7.1 The nature of the multiple components

The relatively high fraction of distant LBGs that have multiple components may tell us important information about their nature of their star-formation and its triggering mechanism. The high fraction of pairs or triplets suggests that the mergers and instabilities that form massive regions of intense star-formation within larger underlying structures may play an important role in $z \sim 5$ LBGs. The observed faint structures surrounding these sources might be indicative of mergers, but could also be structure within the light distribution of a single larger object. There is currently no direct evidence to favour either scenario.

An appropriate way to understand the nature of $z \sim 5$ LBGs may be through analogy with a local population. Overzier et al. (2008) have studied nearby analogues of LBGs – Lyman Break galaxy analogues or LBAs. These LBG analogues were chosen to have properties similar to $z \sim 3$ LBGs, namely, $L_{FUV} > 10^{10.3} L_{\odot}$ and $I_{FUV} > 10^9 L_{\odot} \text{ kpc}^{-2}$. Thus they mimic the high UV luminosities and intensities observed in $z \sim 3$ LBGs. Overall, the LBAs appear to be similar to the $z \sim 5$ LBGs, perhaps more so than the $z \sim 3$ LBGs they were chosen to mimic. Their total stellar masses are between 10^9 and $10^{10} M_{\odot}$, close to the typical masses of bright (brighter than L^*) $z \sim 5$ LBGs (Verma et al. 2007), and low metallicities and similar spectral slopes (§ 5.1, and § 5.2, § 5.3). Their UV luminosities are typically a factor of a few to 10 times lower (λP_{λ} for $\lambda = 1900 \text{ \AA}$) than our sample. Both the small scale clustering properties and the internal kinematics of the LBAs suggest a merger or interaction origin for the intense star-formation observed in these systems (Basu-Zych et al. 2009a,b). Given

the apparent similarities, a detailed comparison seems warranted.

Overzier et al. (2008) find that the clumps of star-formation, or SSBs, in the LBAs, have mass surface densities of $10^{2-3} M_{\odot} \text{ pc}^{-2}$ over radii of $\sim 100 \text{ pc}$, with typically one to more than 10 large SSBs per galaxy. Such systems would be unresolved at $z \sim 5$ in any of our datasets. The half-light radii of the galaxies themselves in the UV or U-band are typically around one kpc. A comparison of this mass surface density with the average surface densities of the Verma et al. (2007) sample (comparable to LBGs studied here) gives a similar average mass surface density ($\approx 6 \times 10^2 M_{\odot} \text{ pc}^{-2}$ over radii of $\sim 1 \text{ kpc}$ or the half light radii of $z \sim 5$ LBGs). In the LBAs, about 30-80% of the total inferred star-formation occurs in such super-starburst (SSB) regions. Thus, the $z \sim 5$ LBGs could be thought of as a “galaxy wide” super-starburst region, with a high density of star-formation that must contribute nearly 100% of the inferred star-formation rates (which would also explain the higher UV luminosities for the $z \sim 5$ LBGs compared to their local analogues). In addition, Overzier et al. (2008) infer ages of the SSBs of about 10-100 Myrs, but formally regard these as upper limits due to complex extinction in the UV and due to the (unknown) contribution of older stars. Interestingly, Verma et al. (2007) derived similar ages from model fits of the bandpass photometry of $z \sim 5$ LBGs. This is all consistent with the picture that the $z \sim 5$ LBGs are possibly a collection of galaxy wide SSBs with a contribution to the total star-formation of nearly 100%.

If the LBGs studied here are analogous to the LBAs, with spatial distributions over one to 5 kpc, with typical separation between components of around 1 kpc, we would only expect to distinguish some of the separate SSB clumps in HST images (*e.g.*, Fig. 7 in Overzier et al. 2008). For the spectroscopically-confirmed galaxies with deep HST imaging, we find 12 that are clearly multiple with an average projected separation of 5.3 kpc and range from separations of one to 16 kpc. For the total photometric sample with deep HST imaging, 14 out of 95 are multiple systems and 16 out of 95 show disturbed morphology (modulo the contamination which should be low Douglas et al. 2009). Taken at face value, the high fraction of multiple or disturbed systems suggests a bias towards spectroscopically confirming such objects. This suggests that the galaxies with multiple components of star formation allow for channels to be cleared of neutral hydrogen, which then provide a long mean free path for the $\text{Ly}\alpha$ photons to escape. Since these galaxies likely drive outflows (Verma et al. 2007), the nature of the ISM may be such to allow the efficient escape of $\text{Ly}\alpha$ photons in analogy with local starburst galaxies (Marlowe, Meurer, & Heckman 1999; Meurer et al. 1992; Atek et al. 2008; Hayes et al. 2007).

8 $Z \sim 5$ SURFACE DENSITY

The average observed surface density of the most reliable photometric sample of galaxies was 0.93 per arcmin² down to $I_{AB} = 26.3$ (see table 2 in paper I), comparable to the surface density observed by Bouwens et al. (2007) to the same flux limit from space-based imaging surveys. However, there is a large variation in the surface density of LBG photo-

Table 4. All confirmed high redshift Lyman break galaxies per field according to the quality of the spectra and the identifying feature.

Field	A		B		Total
	Ly α	break	Ly α	break	
J1037.9-1243		2		1	3
J1040.7-1155	7	2	1	1	11
J1054.4-1146		1		2	3
J1054.7-1245	11	4	1	8	24
J1103.7-1245	3			2	5
J1122.9-1136	2	1			3
J1138.2-1133	5			1	6
J1216.8-1201	2	2			4
J1227.9-1138	2	2			4
J1354.2-1230	3	2			5

metric candidates and spectroscopically confirmed objects between individual fields. Table 4 show this variation in the number of spectroscopically confirmed objects. As expected, the number of confirmed galaxies in each field broadly correlates with the number of photometric candidates. A factor of 8 is observed between the richest and poorest LBG candidate fields and those with the most and least spectroscopic identifications, beyond that expected from cosmic variance predictions (Trenti & Stiavelli 2008).

One possible explanation of the observed variation is the changing effective area of each field. However, with variations in area of less than 10% and no correlation with the density of candidates and confirmed LBGs suggests that this cannot account for the differences.

Alternatively, the presence of foreground clusters in each field (the original subject of the majority of the imaging by the ESO large program EDisCS, (White et al. 2005)) could be distorting the source plane and affecting the probed volume (Clowe et al. 2006). Given the steep nature of the faint-end of the $z \sim 5$ LBG luminosity function (Douglas et al. 2009; Bouwens et al. 2007), the number density of candidates could increase significantly with the flux boosting effect of lensing. As the area of each field affected by strong lensing is small, this is unlikely to be the cause of the observed number variation. There are also no objects observed with highly distorted or elongated morphologies, suggesting strong lensing in the deep images. Although the effects of weak lensing cover a larger proportion of the field, the subsequent distortion effects are small and do not significantly alter the probed volume. There is also no correlation seen between the number of candidates and confirmed LBGs and the velocity dispersion, and hence mass, of the identified foreground clusters. Therefore it is unlikely that the lensing effects of foreground structures are causing the observed differences in LBG surface densities. It is far more likely that these fields are probing truly overdense areas of the universe. The most compelling evidence for this is the variation from a smooth redshift distribution seen in the spectroscopic results of two of the individual fields and is discussed in the next section.

8.1 Spectroscopically confirmed overdense fields

Out of the ten survey fields, two showed strong spectroscopic evidence of large scale structure. In fields J1040.7-1155 and J1054.7-1254 there are clear spikes in the redshift distributions at $z = 5.15$ and $z = 5.0$ respectively, with six or more galaxies lying within a 0.1 redshift bin, which is equivalent to a co-moving distance of around 50Mpc. The redshift distributions for these two fields are shown figures 16 and 19 for J1040.7-1155 and J1054.7.1245 respectively. The red dashed line indicates the distribution of grade A galaxies, the blue dotted line shows the distribution of all grade A and B galaxies, and the black line shows the night sky emission spectrum for the redshift of Ly α . The total redshift distribution of all confirmed galaxies predicts, at most, 1.3 galaxies per 0.1 redshift bin for an individual field.

8.1.1 J1040.7-1155

This field contains the third largest photometric sample of high redshift galaxy candidates out of the ten survey fields, with 25 candidates in the photometric sample (paper I) and 11 high redshift spectroscopic confirmations (grade A and B). Given the size of the photometric sample, a similarly high number of spectroscopic confirmations would be expected. In the redshift distribution there is a clear peak of objects between $5.11 < z < 5.21$, a 6σ overdensity when compared to the spectroscopic statistics of the survey as a whole (with the boundaries of the redshift bins tuned to give the largest peak). Figure 16 shows this peak. Only line emitters with redshift determinations accurate to within $300\text{--}400 \text{ km s}^{-1}$ populate the redshift spike strengthening its identification as a real feature. It cannot be explained as an artifact created by the uncertainty in a Lyman break overlying skyline residual noise. Figure 17 shows the spatial distribution of the galaxies in the redshift spike across the field. Although the galaxies are spread across the field and are not concentrated in one region, it is still probable that they are part of the same structure. The closest pair of grade A galaxies in the field are 7.3Mpc apart, with a furthest extent of 43.7Mpc for the spectroscopically confirmed grade A members of the cluster, where the distances are co-moving in three dimensions. The co-moving dimensions of the surveys fields are typically 27 by 27Mpc in the plane of the sky and probing a redshift interval of one, equivalent to 525Mpc.

The spectra of the galaxies constituting this redshift spike are typical of the line emitting sample as a whole. Similarly, the morphologies and colours of the galaxies within the redshift spike are typical of the sample.

8.1.2 J1054.7-1245

This field contains the most photometric high redshift candidates (45 candidates in paper I), and was expected to produce the largest number of spectroscopic confirmations. Within the spectroscopic identification of 24 high redshift galaxies (grade A and B), there is significant spike at $z = 5.0$ within $\delta z = 0.1$, containing six times more galaxies than expected over such a redshift range (grade A only), see figure 19. The spike includes a close pair with a separation large enough to be individually spatially resolved in the spectrum.

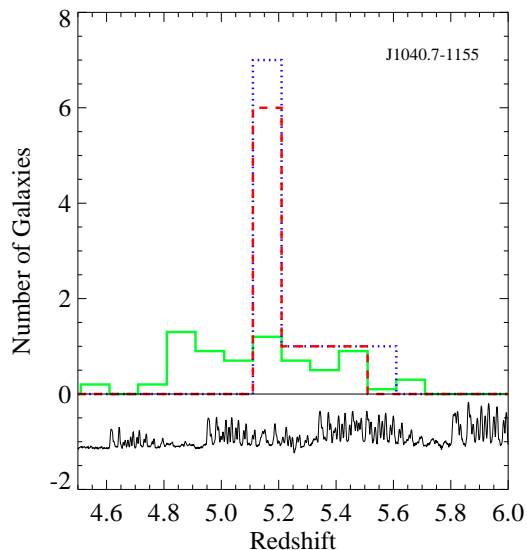


Figure 16. Field J1040.7-1155: The redshift distribution of grade A confirmed galaxies is shown by the dashed red line and the distribution of all confirmed galaxies (grade A and B) is shown by the dotted blue line binned with the same parameters as the individual field data. The solid green line is the total redshift distribution averaged over the ten survey fields. The sky emission spectrum offset from zero at the redshift of $\text{Ly}\alpha$ is shown by the solid black line.

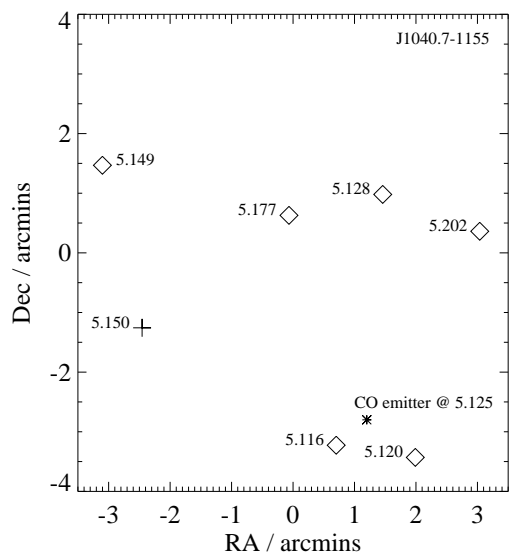


Figure 17. Spatial distribution of spectroscopically confirmed grade A galaxies (diamonds) and grade B galaxies (crosses), which populate the redshift spike, across the field J1040.7-1155. Coordinates are relative to the field centre. The asterisk denotes the position of the Stanway et al. (2008a) CO source discussed in the text.

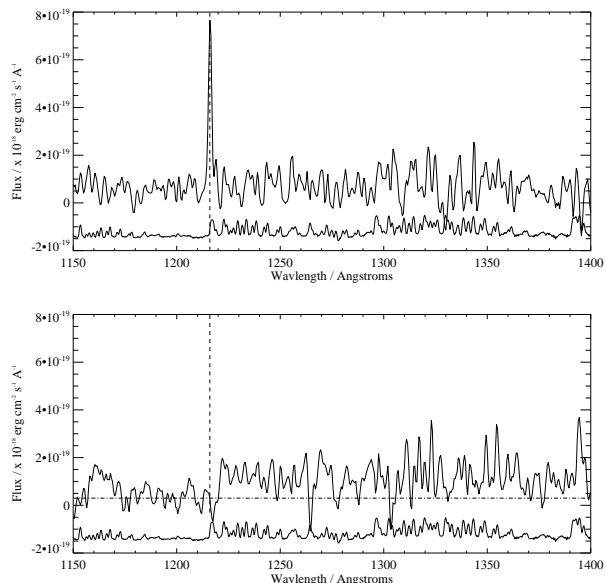


Figure 18. One dimensional spectra of two LBGs separated by $1.1''$ or 7kpc on the sky. The sky spectrum at this redshift is plotted below each spectrum and the location of $\text{Ly}\alpha$ at $z = 4.951$ is shown.

This pair was identified as a $\text{Ly}\alpha$ emitter and break-only galaxy as shown in figure 18. When both grades of spectroscopic confirmations of high redshift galaxies are included, this overdensity contains nine galaxies. If we include objects between $z = 4.95$ and $z = 5.15$, i.e. $\delta z = 0.2$, 17 grade A and B galaxies are included. However this redshift range is much larger than that expected for a cluster of galaxies or any other bound structure. The broad nature of this spike may suggest we are observing a filamentary structure end-on. Again the overdensity is mainly determined by line emitters, a reflection of the greater fraction of line emitting galaxies confirmed compared to break-only galaxies in this field.

The galaxies in the redshift spike are spatially distributed over a smaller fraction of the field than those in J1040.7-1155. They are clustered to one side of the 7×7 arcminute field, as shown in figure 20. The closest grade A galaxy pair has a co-moving separation of 670 kpc (excluding the very close pair), with the overdensity of galaxies covering 27 Mpc (co-moving distance between furthest grade A confirmed galaxies in three dimensions). Again, the spectra, colours and morphologies of the galaxies within the redshift spike are typical of the sample as a whole.

8.2 The Nature of the Large Scale Structure

As discussed above, two of the ten survey fields show evidence of large scale structure in the form of spikes in their redshift distributions. Such overdensities could be a forming cluster, sheet or filament being probed in these fields. Given that across the survey as a whole zero to one sources per 0.1 in redshift are expected, the identification of two fields with very clear overdensities of many times this expected number is highly significant. However, given the stochastic

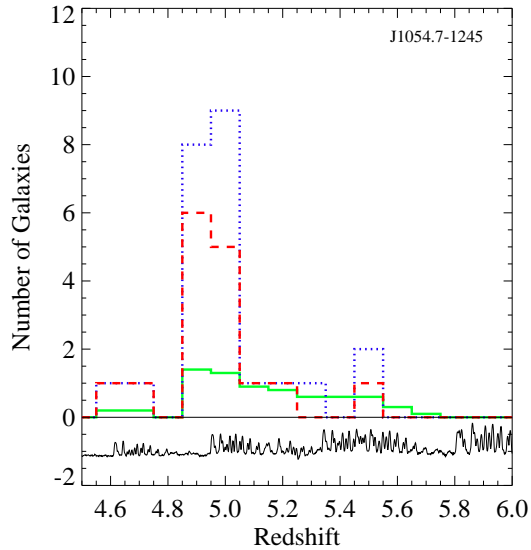


Figure 19. Field J1054.7-1245: The redshift distribution of grade A confirmed galaxies is shown by the dashed red line and the distribution of all confirmed galaxies (grade A and B) is shown by the dotted blue line. The solid green line is the total redshift distribution averaged over the ten survey fields binned with the same parameters as the individual field data. The sky emission spectrum offset from zero at the redshift of $\text{Ly}\alpha$ is shown by the solid black line.

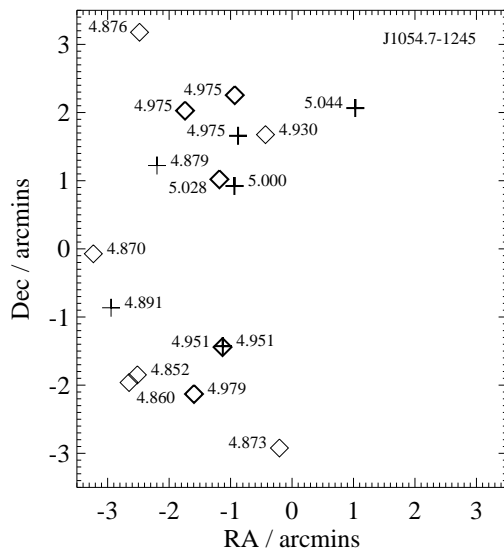


Figure 20. Spatial distribution of spectroscopically confirmed grade A galaxies (diamonds) and grade B galaxies (crosses), which populate the two 0.1 redshift spikes (distinguished by bold symbols), across the field J1054.7.1245. Coordinates are relative to the field centre.

properties of LBGs (Verma et al. 2007), the nature of these overdensities is not immediately clear.

As the typical star-formation lifetime of high redshift LBGs is a few tens Myrs (assuming the majority of the galaxies within the overdensities are young, Verma et al. 2007), the apparent coordination or synchronisation of these short-lived star-bursts over the entire field needs explanation. Given the distances between the galaxies within the redshift overdensities, it is highly unlikely that these galaxies are dynamically bound or interacting sufficiently to have a common starformation trigger. Assuming the young ages of these galaxies predicted by Verma et al. (2007), <45 Myrs, it is likely that the galaxies have only travelled 50 kpc, outside the Hubble flow, in their lifetime (assuming the galaxy is travelling at 1000 km s^{-1}). This suggests that if two galaxies are more than 100 kpc apart, it is unlikely that they have interacted. With the closest pair of galaxies (in field J1054.7-1245) separated by 670 kpc (co-moving distance in three dimensions), the star formation observed cannot be connected. This limited interaction region is reflected in the high resolution imaging of the HST data. It was found that many objects detected in the ground based data were in fact multiple systems, at most 16 kpc apart and are subsequently close enough to potentially have star formation triggered by the mutual interaction.

The apparent synchronisation of the relatively short-lived starbursts is likely to be an illusion for the above reasons. A more plausible explanation for the overdensity of objects undergoing a relatively short-lived phenomenon is that there is far more baryonic material in the large-scale structure that hosts these galaxies than is visible in the rest-frame UV. At any one time a small fraction of this material is visible as unobscured UV-bright starburst episodes lasting a few tens of Myrs. If one were to wait a few tens of millions of years and re-observe the region, the large scale structure would still be marked out by an overdensity of UV-luminous starbursts, but probably different ones to those seen today. Therefore, there is no synchronisation of the starbursts, just a high probability that several regions of the large-scale structure will be ‘on’ at any one time. One way to try to detect this ‘dark’ material connecting the observed systems, is to look for line or continuum emission, such as carbon or CO emission lines, from gas within the structure, in the millimetre and submillimetre regimes. Such an experiment was carried out in a 2 arcminute diameter region centred between two LBGs with concurrent redshifts in one of the overdense fields (Stanway et al. 2008a). Although none of the optically identified LBGs were detected in the 37.7 GHz band, a faint CO(2-1) emission line was detected at the same redshift as the optically identified overdensity (and subsequently reconfirmed in independent data, Stanway et al., in prep), shown in figure 17. With no optical or near-infrared counterpart in the available imaging and a inferred molecular hydrogen gas mass of $2 \times 10^{10} M_{\odot}$ this line emitter is tracing previously undetectable baryonic mass.

The assumption that there is a large reservoir of undetected material in the structures is consistent with the work of Thomas et al. (2005), which, through analysis of fossil populations in nearby galaxies, determined that massive galaxies found in high density environments formed the majority of their stars at $z > 4$. Further support for such old star formation in massive galaxies is provided by

the distant red galaxy (DRG) population at $z = 2 - 3$. Labbé et al. (2005) observed DRGs which had UV to $8\mu\text{m}$ spectral energy distributions fitted best by an old stellar population with very little current star formation. From the Bruzual & Charlot (2003) models used, they infer that the majority of the stellar mass was in place by $z \sim 5$ or earlier (depending on the metallicity assumed). Similarly, Panter et al. (2007) report that the most massive systems seen today formed the majority of their stars at $z > 4$, from analysis of 30,000 galaxy spectra from the Sloan Digital Sky Survey. Stark et al. (2007) also predict that a significant fraction of the mass at $z \sim 5$ is not being observed in Lyman break galaxy surveys. Assuming that galaxies seen here at $z \sim 5$ are mainly young, the typical stellar mass found by Verma et al. (2007) was a few $10^9 M_\odot$. If this mass is applied to the galaxies in the redshift overdensities, and it is assumed that over time they will merge into one of the most massive systems today (a best-case scenario to accumulate the most mass), the observed stellar mass at $z = 5$ would only account for around 2% of the final baryonic mass of a massive galaxy at $z = 0$. Although the structures may extend beyond the 44 arcmin^2 field of view of the imaging or a fraction of the galaxies could be older and more massive than typical of the population, there is still large fraction of the mass unaccounted for.

The apparent problem of starburst synchronisation can be avoided if the galaxies in the overdensities have older stellar populations with longer-lived starbursts than are typical of the population as a whole. Although the majority of LBGs at $z \sim 5$ studied by Verma et al. (2007) are young, a number of older, more massive systems were identified. Similarly, individual relatively bright objects at $z \sim 6$ have been observed by Yan et al. (2006) and Eyles et al. (2005) and were found to have older and more massive stellar populations. Finding individual old galaxies suggests that the formation and assembly of massive galaxies had already started by $z \sim 10$. As such sources are expected to be in the minority of the $z \sim 5$ population, discovering a connected system of old galaxies would pose significant problems for our understanding of galaxy and structure formation.

To distinguish between these two scenarios, multiband SED fitting of the sources is required. With the additional deeper near infrared and Spitzer IRAC imaging that is currently being added to this extensive data set, it will be possible to probe the rest-frame UV to optical spectral energy distributions of these galaxies and determine whether they have young or old stellar populations.

9 $Z \sim 6$ GALAXIES

As noted previously in section 2.2, the imaging dataset of V , R , I , z , J and K_s -bands can be used to select high redshift objects at $z \sim 6$ using an $I_{AB} - z_{AB}$ colour cut. A total of 73 candidates were observed spectroscopically with an $I_{AB} - z_{AB} > 1.3$ and non detections in the V and R -bands. From this sample two objects were confirmed to be galaxies at $z \sim 6$.

A galaxy with an observed $z_{AB} = 25.7$ and a colour of $I_{AB} - z_{AB} = 1.4$ was confirmed to be at $z = 5.99$ with strong line emission and weak continuum at longer wavelengths but none at shorter wavelengths. With a $\text{Ly}\alpha$ flux of 1.9×10^{-17}

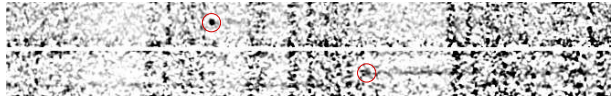


Figure 21. 2D spectra of the LBGs at $z = 5.99$ (top frame) and $z = 6.41$ (bottom frame). Both show the spectral region between 7800\AA and 9800\AA .

$\text{ergs cm}^{-2} \text{s}^{-1}$, the rest-frame equivalent width is 46\AA measured using the same method as the $z \sim 5$ galaxies (section 6). The second galaxy was confirmed with a weaker $\text{Ly}\alpha$ line and continuum break at $z = 6.41$. This galaxy was observed to have $z_{AB} = 24.9$ and a colour of $I_{AB} - z_{AB} > 2$. The line flux and rest-frame equivalent width of this emission are $9.4 \times 10^{-18} \text{ ergs cm}^{-2} \text{s}^{-1}$ and 8\AA respectively.

Of the other candidates observed, 8 were at low redshift and the remaining 63 had signal-to-noise too low to be able to identify the sources. The large number of unidentified objects is unsurprising given the decreasing response of the FORS2 instrument beyond 9000\AA . With better instrumental responses and a wider range of wavelengths uncluttered by sky lines at shorter wavelengths, it is markedly easier to study $z \sim 5$ galaxies than their higher redshift counterparts, even those observed when the Universe was just 200-250 Myrs older.

10 CONCLUSIONS

We have carried out a large spectroscopic survey of 10 widely-separate fields targeting $z \sim 5$ LBGs. The candidates were selected using deep optical imaging combined with a colour selection tuned to identify the Lyman Break at $z \sim 5$. A total of 70 LBGs at $4.6 < z < 5.6$ have been identified, 38 galaxies with $\text{Ly}\alpha$ emission ranging in strength from 2.6×10^{-18} to $7 \times 10^{-17} \text{ erg cm}^{-2} \text{s}^{-1}$ (luminosities between 10^{42} and $10^{43} \text{ erg s}^{-1}$), and 32 were identified by their strong continuum break at a rest wavelength of 1216\AA . An additional two galaxies were confirmed to be at $z \sim 6$, selected for their red $I - z$ colours. A comparison of the equivalent width distribution of the $\text{Ly}\alpha$ emission of the confirmed $z \sim 5$ LBGs and that of $z \sim 3$ LBGs from Shapley et al. (2003) shows that the confirmed higher redshift objects are twice as likely to have large ($> 20\text{\AA}$) equivalent width $\text{Ly}\alpha$ emission. Just over half of the $z \sim 5$ objects have $\text{Ly}\alpha$ lines stronger than this. The largest measured equivalent width is $W_o = 122 \pm 18\text{\AA}$. However, including plausible corrections for the spectroscopically-unconfirmed objects which are nevertheless at these redshifts removes any significant difference in the fraction of sources with large ($> 20\text{\AA}$) equivalent widths in both samples.

A comparison of the average optical spectra and average $I_{AB} - K_{AB}$ colours of LBGs with and without detectable $\text{Ly}\alpha$ emission showed that the break-only galaxies had a redder colour and hence steeper rest-frame UV continuum slope than the line emitting galaxies. It is difficult for stellar age differences alone to explain this difference given the statistics on the ages of sources from Verma et al. (2007). It can be straightforwardly explained by variations in reddening (a difference of $E(B-V) \sim 0.2$ assuming a Calzetti et al. (2000) reddening law can account

for the difference in colours) and/or metallicity between the two subsamples, though age could clearly also play a part. A similar, but smaller colour difference is seen between samples of line-emitting and break-only LBGs at lower redshifts.

If the local correlation between UV-slope and metallicity is assumed to be applicable at high redshifts, a typical $z \sim 5$ LBG has a metallicity of approximately 0.1-0.2 of the solar value, approximately a third that of the metallicity of $z \sim 3$ LBGs.

The morphology of the confirmed $z \sim 5$ galaxies was studied using high resolution HST/ACS images and was found to be similar to that seen in larger photometric samples with a typical half-light radius of $0.15''$ or 1 kpc. However, a higher fraction of multiple and disturbed systems was observed (16 out of 18 LBGs) suggesting such systems are more likely to be confirmed spectroscopically, with a greater incidence of Ly α emission. A comparison of the multiple $z \sim 5$ systems with local analogues of LBGs suggests that the components identified in the high resolution imaging could be either super-starburst regions within a larger structure with a surface brightness below the detection limit, or part of merging objects.

The surface densities of LBGs in two of the ten fields are substantially higher than in the rest. In both cases the fields contain a clear excess of LBGs over a narrow range in redshift ($z = 5.05 \pm 0.1$ and $z = 5.15 \pm 0.05$). Although these are coherent structures, they may extend beyond the observed fields (with scale sizes of 20-50 Mpc) and cannot be bound or virialised systems. Given the distances between the LBGs within these excesses and the expected short (no more than a few tens of Myr) timescale for typical $z \sim 5$ LBGs, the excess of systems cannot be caused by gravitational interactions between the LBGs triggering starbursts. It is more likely that the LBGs are comparatively rare UV-luminous markers for a much larger mass (both baryonic and dark) of UV-dark material in these volumes.

In addition to the survey for $z \sim 5$ LBGs, we use the same photometric data to carry out a comparatively limited search for $z \sim 6$ LBGs by looking for objects with spectral breaks between the I and z -band images. We confirmed two such galaxies, one at $z = 5.99$ with a Ly α line flux of 1.9×10^{-17} erg cm $^{-2}$ s $^{-1}$ and $z_{AB} = 25.7$ and another at $z = 6.41$ with a much weaker Ly α line (9.4×10^{-18} erg cm $^{-2}$ s $^{-1}$), but considerably brighter continuum ($z_{AB} = 24.9$).

ACKNOWLEDGEMENTS

LSD acknowledges support from P2I. ERS acknowledges support from STFC. Based on observations made with ESO Telescopes at the La Silla and Paranal Observatory under programme IDs 166.A-0162 and 175.A-0706. Also based on observations made with the NASA/ESA Hubble Space Telescope, obtained at the Space Telescope Science Institute, which is operated by the Association of Universities for Research in Astronomy, Inc., under NASA contract NAS 5-26555. These observations are associated with program 9476. We thank the members of the EDisCS collaboration for creating an imaging dataset with a usefulness far beyond their original intent. The astronomical table manipulation and plotting software TopCat (Taylor 2005) was used in the anal-

ysis of this data. The Dark Cosmology Centre is funded by the Danish National Research Foundation.

REFERENCES

- Ando M., Ohta K., Iwata I., Akiyama M., Aoki K., Tamura N., 2007, PASJ, 59, 717
- Ando M., Ohta K., Iwata I., Watanabe C., Tamura N., Akiyama M., Aoki K., 2004, ApJ, 610, 635
- Appenzeller I., et al., 1998, Msngr, 94, 1
- Atek H., Kunth D., Hayes M., Östlin G., Mas-Hesse J. M., 2008, A&A, 488, 491
- Basu-Zych A. R., et al., 2009, ApJ, 699, 1307
- Basu-Zych A. R., et al., 2009, ApJ, 699, L118
- Bertin E., Arnouts S., 1996, A&AS, 117, 393
- Bouwens R. J., Illingworth G. D., Blakeslee J. P., Franx M., 2006, ApJ, 653, 53
- Bouwens R. J., Illingworth G. D., Franx M., Ford H., 2007, ApJ, 670, 928
- Bremer M. N., Lehnert M. D., Waddington I., Hardcastle M. J., Boyce P. J., Phillipps S., 2004, MNRAS, 347, L7
- Bruzual G., Charlot S., 2003, MNRAS, 344, 1000
- Calzetti D., Armus L., Bohlin R. C., Kinney A. L., Koornneef J., Storchi-Bergmann T., 2000, ApJ, 533, 682
- Clowe D., et al., 2006, A&A, 451, 395
- Conselice C. J., Arnold J., 2009, MNRAS, 397, 208
- Dawson S., Rhoads J. E., Malhotra S., Stern D., Wang J., Dey A., Spinrad H., Jannuzi B. T., 2007, ApJ, 671, 1227
- Desai V., et al., 2007, ApJ, 660, 1151
- Dunne L., Eales S., Edmunds M., Ivison R., Alexander P., Clements D. L., 2000, MNRAS, 315, 115
- Douglas, L. S., Bremer, M. N., Stanway, E. R., & Lehnert, M. D. 2007, MNRAS, 376, 1393
- Douglas, L. S., Bremer, M. N., Stanway, E. R., Lehnert, M. D., & Clowe, D. MNRAS accepted
- Dow-Hygelund, C. C., et al. 2005, ApJ, 630, L137
- Dow-Hygelund, C. C., et al. 2007, ApJ, 660, 47
- Erb D. K., Steidel C. C., Shapley A. E., Pettini M., Reddy N. A., Adelberger K. L., 2006, ApJ, 646, 107
- Eyles, L. P., Bunker, A. J., Stanway, E. R., Lacy, M., Ellis, R. S., & Doherty, M. 2005, MNRAS, 364, 443
- Fullmer L., Lonsdale C. J., 1989, IRASG, 0
- Hayes M., Östlin G., Atek H., Kunth D., Mas-Hesse J. M., Leitherer C., Jiménez-Bailón E., Adamo A., 2007, MNRAS, 382, 1465
- Heckman T. M., Robert C., Leitherer C., Garnett D. R., van der Rydt F., 1998, ApJ, 503, 646
- Heckman T. M., 2001, ASPC, 240, 345
- Hu, E. M., Cowie, L. L., Capak, P., McMahon, R. G., Hayashino, T., & Komiyama, Y. 2004, AJ, 127, 563
- Knapp, G. R., et al. 2004, AJ, 127, 3553
- Labbé, I., et al. 2005, ApJ, 624, L81
- Lehnert M. D., Heckman T. M., 1996, ApJ, 472, 546
- Lehnert, M. D., & Bremer, M. 2003, ApJ, 593, 630
- Leitherer C., Heckman T. M., 1995, ApJS, 96, 9
- Mannucci F., et al., 2009, arXiv, arXiv:0902.2398
- Maraston, C. 2005, MNRAS, 362, 799
- Marlowe A. T., Meurer G. R., Heckman T. M., 1999, ApJ, 522, 183
- Meurer G. R., Heckman T. M., Lehnert M. D., Leitherer C., Lowenthal J., 1997, AJ, 114, 54

- Meurer G. R., Freeman K. C., Dopita M. A., Cacciari C., 1992, *AJ*, 103, 60
- Nesvadba N. P. H., et al., 2006, *ApJ*, 650, 661
- Nesvadba N. P. H., Lehnert M. D., Davies R. I., Verma A., Eisenhauer F., 2008, *A&A*, 479, 67
- Neufeld D. A., 1991, *ApJ*, 370, L85
- Oke, J. B., & Gunn, J. E. 1983, *ApJ*, 266, 713
- Ouchi, M., et al. 2004, *ApJ*, 611, 660
- Overzier R. A., et al., 2008, *ApJ*, 677, 37
- Panther, B., Jimenez, R., Heavens, A. F., & Charlot, S. 2007, *MNRAS*, 378, 1550
- Pettini M., Shapley A. E., Steidel C. C., Cuby J.-G., Dickinson M., Moorwood A. F. M., Adelberger K. L., Giavalisco M., 2001, *ApJ*, 554, 981
- Pentericci, L., Grazian, A., Fontana, A., Salimbeni, S., Santini, P., de Santis, C., Gallozzi, S., & Giallongo, E. 2007, *A&A*, 471, 433
- Shapley, A. E., Steidel, C. C., Pettini, M., & Adelberger, K. L. 2003, *ApJ*, 588, 65
- Stanway, E. R., Bremer, M. N., Davies, L. J. M., Birkinshaw, M., Douglas, L. S., & Lehnert, M. D. 2008a, *ApJ*, 687, L1
- Stanway, E. R., Bremer, M. N., & Lehnert, M. D. 2008b, *MNRAS*, 385, 493
- Stanway E. R., Bremer M. N., Lehnert M. D., Eldridge J. J., 2008, *MNRAS*, 384, 348
- Stanway, E. R., et al. 2007, *MNRAS*, 376, 727
- Stanway, E. R., Bunker, A. J., McMahon, R. G., Ellis, R. S., Treu, T., & McCarthy, P. J. 2004, *ApJ*, 607, 704
- Stark, D. P., Bunker, A. J., Ellis, R. S., Eyles, L. P., & Lacy, M. 2007, *ApJ*, 659, 84
- Steidel, C. C., Adelberger, K. L., Giavalisco, M., Dickinson, M., & Pettini, M. 1999, *ApJ*, 519, 1
- Taylor, M. B., in Shopbell P., Britton M., Ebert R., eds, *ASP Conf. Ser. Vol. 347, ADASS XIV. Astron Soc. Pac.*, San Francisco, p. 29
- Thomas, D., Maraston, C., Bender, R., & Mendes de Oliveira, C. 2005, *ApJ*, 621, 673
- Trenti M., Stiavelli M., 2008, *ApJ*, 676, 767
- Vanzella E., et al., 2005, *A&A*, 434, 53
- Vanzella E., et al., 2009, *ApJ*, 695, 1163
- Verma, A., Lehnert, M. D., Förster Schreiber, N. M., Bremer, M. N., & Douglas, L. 2007, *MNRAS*, 377, 1024
- White, S. D. M., et al. 2005, *A&A*, 444, 365
- Yan H., Dickinson M., Giavalisco M., Stern D., Eisenhardt P. R. M., Ferguson H. C., 2006, *ApJ*, 651, 24